

# Improved quantum pair potentials for correlated Coulomb systems

A.V. Filinov<sup>1</sup>, V.O. Golubnychiy<sup>2</sup>, M. Bonitz<sup>1</sup>, W. Ebeling<sup>3</sup>, and J.W. Dufty<sup>4</sup>

<sup>1</sup>*Institut für Theoretische Physik und Astrophysik,*

*Christian-Albrechts-Universität Kiel, Leibnizstr. 15, D-24098 Kiel, Germany*

<sup>2</sup>*Fachbereich Physik, Universität Rostock, Universitätsplatz 3, D-18051 Rostock, Germany*

<sup>3</sup>*Institut für Physik, Humboldt-Universität Berlin, Invalidenstrasse 110 D-10115 Berlin and*

<sup>4</sup>*University of Florida, Department of Physics, PO Box 118440, Gainesville FL 32611-8440*

Effective two-body potentials for electron-ion plasmas are analyzed. Such potentials which have been previously derived by Kelbg and others capture the basic quantum diffraction effects and are exact in the weak coupling limit. Moreover, using path integral Monte Carlo methods, they can be applied to strongly coupled plasmas which include bound states. We investigate the accuracy of the diagonal Kelbg potential as well as the off-diagonal Kelbg potential by comparison with accurate numerical solutions of the off-diagonal two-particle Bloch equation. Results for the energies and pair distribution functions are presented. A significant improvement is achieved by correcting the potential value at zero particle separation, and analytical expressions for improved interaction potential between electrons and protons and electrons with parallel and antiparallel spins are obtained. Further, application of the quantum pair potentials in path integral Monte Carlo and in classical molecular dynamics simulations of dense hydrogen are presented. Finally, we point out an interesting relation between the quantum potential and effective potentials used in density functional theory.

## I. INTRODUCTION

The behavior of strongly correlated Coulomb systems at high pressure is of growing importance in many fields, including shock and laser plasmas, astrophysics, metals, semiconductors, dusty plasmas etc., see Refs. [1, 2, 3, 4, 5, 6] for an overview. In particular, the thermodynamic properties of hot dense plasmas are essential for the description of plasmas generated by strong lasers [5]. Further, among the phenomena of current interest are the high-pressure compressibility of deuterium [7], metalization of hydrogen [8] and the hypothetical plasma phase transition, e.g. [9, 10, 11, 12, 13, 14, 15] which occur in situations where both *interaction and quantum effects* are relevant.

There has been significant progress in recent years in studying these dense partially ionized systems analytically and numerically, see e.g. [1, 2, 4, 13, 16, 17] for an overview. Analytical methods typically use a chemical picture where electrons, ions and bound states such as atoms and molecules are treated as independent species, and the chemical composition (degree of ionization) is computed from a mass action law (nonideal Saha equation). These methods are based on perturbation expansions in the coupling strength and are thus limited to regions of small coupling parameters (see below),  $\Gamma < 1$  or  $r_s < 1$ . Further, the mass action law becomes increasingly inaccurate in the region where the electrons are degenerate (uncertainty in the mass action constants). Also, during rapid pressure ionization around the Mott density the distinction between free and bound particles is an open problem.

The alternative approach to correlated Coulomb systems are simulations such as Monte Carlo or molecular dynamics (MD) which have no limitations with respect to the coupling strengths. However, standard MD is limited

to classical systems [18]. Nevertheless it can be extended to weakly degenerate plasmas by replacing the Coulomb potential by effective quantum pair potentials, such as proposed by Kelbg [20], Deutsch [21], Klakow, Toepffer and Reinhard [16] and many others, e.g. [22, 23, 24]. However, no rigorous assessment of the accuracy of these simulations has been reported yet, which is one of the aims of this paper. Similarly, this question is important for path integral Monte Carlo simulations (PIMC). Here, use of the Trotter formula allows to map a strongly degenerate and/or strongly coupled system to a weakly correlated nearly classical one. This further allows to reduce the many-body problem to a two-particle one which can be solved either exactly or, by using quantum pair potentials, e.g. [28, 29]. The latter case is particularly interesting due to the use of analytical potentials which themselves have physical relevance, explicitly containing quantum effects. Thus, again, the question of the quality of the effective potential arises which will be addressed below, extending our previous work [30].

This paper is organized as follows: In Section II a derivation of effective quantum potentials is outlined. It is demonstrated that, in the weak coupling limit, this potential leads exactly to the off-diagonal Kelbg potential the properties of which are being discussed and compared to its commonly used diagonal limit and to other approximations for quantum potentials. In Section III we outline two methods for a direct solution of the off-diagonal two-body Bloch equation which are then used in Section IV for numerical comparison with the analytical quantum potentials and allow to assess the accuracy of the latter. After this, the exact solutions are used to derive improved diagonal Kelbg potentials by introducing a single temperature dependent fit parameter which replaces the ideal electron DeBroglie wave length by a proper generalization due to correlation effects. Further,

an analysis of the accuracy of PIMC simulations, using respectively the diagonal and off-diagonal Kelbg potentials, is given. Section V describes an application of the improved Kelbg potentials to classical molecular dynamics simulations of dense hydrogen. Comparing the results to those of PIMC simulations allows us to conclude that use of the improved Kelbg potential allows to significantly extend the range of applicability of classical MD to the region of partial ionization and to temperatures as low as approximately on third of the binding energy. Section VI discusses another field of potential applicability of the quantum potentials – density functional theory. Finally, Section VII concludes the paper with a discussion.

## II. EFFECTIVE QUANTUM PAIR POTENTIALS

In this section we derive an approximation for the high-temperature *two-particle* density matrix of an  $N$ -particle charged particle system consisting of electrons and ions in thermodynamic equilibrium. Further, we demonstrate that the proper choice of an analytical effective quantum pair potential is given by the Kelbg potential [20, 41]. This result is applicable to the full *many-particle* system at sufficiently high temperature. Then, the  $N$ -particle density matrix can be expanded in terms of 2-particle, 3-particle etc. contributions among which the first,  $\rho_{ij}$ , gives the dominant contribution.

### A. Two-body Bloch equation. Off-diagonal and diagonal Kelbg potential

The equilibrium pair density matrix at a given inverse temperature  $\beta = 1/k_B T$  is the solution of the two-particle Bloch equation

$$\frac{\partial}{\partial \beta} \rho(\mathbf{r}_i, \mathbf{r}_j, \mathbf{r}'_i, \mathbf{r}'_j; \beta) = -\hat{H} \rho(\mathbf{r}_i, \mathbf{r}_j, \mathbf{r}'_i, \mathbf{r}'_j; \beta),$$

$$\hat{H} = \hat{K}_i + \hat{K}_j + \hat{U}(\mathbf{r}_i, \mathbf{r}_j, \mathbf{r}'_i, \mathbf{r}'_j). \quad (1)$$

Methods for solution of the Bloch equation (1) will be considered in Sec. III. Here, we concentrate on the available analytical solutions in the limit of weak coupling. If the interaction is weak, Eq. (1) can be solved by perturbation theory with the following representation for the two-particle density matrix

$$\rho_{ij} = \frac{(m_i m_j)^{3/2}}{(2\pi\hbar\beta)^3} \exp\left[-\frac{m_i}{2\hbar^2\beta}(\mathbf{r}_i - \mathbf{r}'_j)^2\right] \times \exp\left[-\frac{m_j}{2\hbar^2\beta}(\mathbf{r}_i - \mathbf{r}'_j)^2\right] \exp[-\beta\Phi^{ij}], \quad (2)$$

where  $i, j$  are particle indices,  $\rho_{ij} \equiv \rho(\mathbf{r}_i, \mathbf{r}_j, \mathbf{r}'_i, \mathbf{r}'_j; \beta)$ , and  $\Phi^{ij}(\mathbf{r}_i, \mathbf{r}_j, \mathbf{r}'_i, \mathbf{r}'_j; \beta)$  is the off-diagonal two-particle effective potential. In the following we will consider application of this result to Coulomb systems. As a result

of first-order perturbation theory we get explicitly, for details see [41]

$$\Phi^{ij}(\mathbf{r}_{ij}, \mathbf{r}'_{ij}, \beta) \equiv e_i e_j \int_0^1 \frac{d\alpha}{d_{ij}(\alpha)} \operatorname{erf}\left(\frac{d_{ij}(\alpha)/\lambda_{ij}}{2\sqrt{\alpha(1-\alpha)}}\right), \quad (3)$$

where  $d_{ij}(\alpha) = |\alpha\mathbf{r}_{ij} + (1-\alpha)\mathbf{r}'_{ij}|$ ,  $\operatorname{erf}(x)$  is the error function,  $\operatorname{erf}(x) = \frac{2}{\sqrt{\pi}} \int_0^x dt e^{-t^2}$ , and  $\lambda_{ij}^2 = \frac{\hbar^2\beta}{2\mu_{ij}}$  with  $\mu_{ij}^{-1} = m_i^{-1} + m_j^{-1}$ . The diagonal element ( $\mathbf{r}'_{ij} = \mathbf{r}_{ij}$ ) of (3) is just the familiar Kelbg potential, given by

$$\Phi^{ij}(x_{ij}) = \frac{e_i e_j}{\lambda_{ij} x_{ij}} \left\{ 1 - e^{-x_{ij}^2} + \sqrt{\pi} x_{ij} [1 - \operatorname{erf}(x_{ij})] \right\} \quad (4)$$

with  $x_{ij} = |\mathbf{r}_{ij}|/\lambda_{ij}$ , and we underline that the Kelbg potential is finite at zero distance reflecting the quantum nature of two-particle interaction at small distances which prevents any divergence. From Eq. (4) it is also clear that quantum effects become dominant (and there the quantum potential deviates from the classical Coulomb potential) at distances  $r_{ij} \lesssim \lambda_{ij}$  given by the thermal DeBroglie wavelength. We will see below that, in interacting systems, this is only a rough approximation, and at strong coupling, the expression for the quantum particle “extension” deviates strongly from  $\lambda_{ij}$  and needs to be generalized.

To obtain a simplified expression for the rather complex quantum potential (3) one can approximate the off-diagonal matrix elements by the diagonal ones. A first possibility is to approximate the integral over  $\alpha$  by the length of the interval multiplied with the integrand in the center (Mittelwertsatz) which leads to the so-called KTR-potential due to Klakow, Toepffer and Reinhard which (in the diagonal approximation) is often used in quasi-classical MD simulations [16]

$$\Phi^{ij}(\mathbf{r}_{ij}, \mathbf{r}'_{ij}, \beta) \equiv \frac{e_i e_j}{d_{ij}(1/2)} \operatorname{erf}\left(\frac{d_{ij}(1/2)}{\lambda_{ij}}\right), \quad (5)$$

where  $d_{ij}(1/2) = \frac{1}{2}|\mathbf{r}_{ij} + \mathbf{r}'_{ij}|$ . Alternatively, the integral can be simplified by taking the off-diagonal Kelbg potential only at the center coordinate,

$$\Phi^{ij}(\mathbf{r}_{ij}, \mathbf{r}'_{ij}, \beta) \approx \Phi^{ij}\left(\frac{|\mathbf{r}_{ij}| + |\mathbf{r}'_{ij}|}{2}, \beta\right). \quad (6)$$

Many authors use the *end-point* approximation (4) for the effective potential  $\Phi^{ij}(\mathbf{r}_{ij}, \mathbf{r}'_{ij}, \beta)$  in the pair density matrix (2) due to the fact that it is very convenient computationally. The pair potential for interparticle interaction simply is replaced by an effective potential which has only a dependence on the radial variables  $|\mathbf{r}_{ij}|$ ,  $|\mathbf{r}'_{ij}|$ . However, most of the accuracy is usually lost in this end-point approximation.

Below we check the accuracy and range of applicability of the Kelbg potential for the case of strong electron-proton correlations. Since the Kelbg potential is obtained

by first order perturbation theory its application is limited to weak coupling,  $\Gamma \lesssim 1$ , where  $\Gamma$  is the ratio of mean potential to kinetic energy. In unbound and bound states of an electron-proton pair this results in the following conditions on temperature

$$\begin{aligned} \Gamma = \frac{e^2}{\bar{r}}/k_B T \lesssim 1 &\Rightarrow k_B T \gtrsim \frac{e^2}{\bar{r}} \\ \Gamma = \text{Ry}/k_B T \lesssim 1 &\Rightarrow k_B T \gtrsim \text{Ry}, \end{aligned} \quad (7)$$

where  $\text{Ry} = \text{Ha}/2 = e^2/2a_B$ , and  $a_B$  is the Bohr radius. For the last case the Kelbg potential (and any of the simplifying approximations) can be only valid for temperatures sufficiently above the atomic binding energy, i.e for the case of hydrogen,  $T \gtrsim \text{Ry}/k_B \approx 158\,000$  K. We address this point in more detail in the next section IV, where ‘exact’ binding energies and pair correlation functions for an electron-proton pair are compared with the results obtained with the potentials (3) and (4).

In the next section we will briefly describe methods that were applied to solve the two-particle problem.

### III. SOLUTION OF THE OFF-DIAGONAL BLOCH EQUATION

There are various ways of computing the ‘exact’ pair density matrix. First, one can use a direct eigenfunction expansion of the density matrix and calculate the contributions from bound and continuum states. This method is particularly useful for the types of potentials where analytic expressions for the continuum wave functions exist. Other cases require a separate calculation for each matrix element  $\rho(\mathbf{r}, \mathbf{r}'; \beta)$  which may be not efficient for numerical simulations with frequent use of the off-diagonal density matrix, such as path integral Monte Carlo. Usually in such type of simulations it is crucial that the off-diagonal density matrix can be quickly evaluated for given initial,  $(\mathbf{r}_i, \mathbf{r}_j)$ , and final,  $(\mathbf{r}_i', \mathbf{r}_j')$ , particle positions. In the present work, to solve this problem, we used two efficient methods – the *matrix squaring technique* [31, 33] and a *variational approach* [34, 35]. We will apply both methods and, therefore, give a brief summary of their main points.

#### A. Matrix squaring technique

The exact off-diagonal pair density matrix can be calculated efficiently by this method introduced by Storer and Klemm [31]. First, the density matrix is factorized into a center-of-mass term and a term that is a function of the relative coordinates only

$$\rho(\mathbf{r}_i, \mathbf{r}_j, \mathbf{r}_i', \mathbf{r}_j'; \beta) = \rho_{\text{cm}}(\mathbf{R}, \mathbf{R}'; \beta) \rho(\mathbf{r}, \mathbf{r}'; \beta), \quad (8)$$

where  $\mathbf{R} = (m_i \mathbf{r}_i + m_j \mathbf{r}_j)/(m_i + m_j)$ , and  $\mathbf{r} = \mathbf{r}_i - \mathbf{r}_j$ , and analogously for  $\mathbf{R}', \mathbf{r}'$ . For the case of spherical symmetry of the interaction potential, the relative pair

density matrix is expanded in terms of partial waves. This expansion reads, for the two- and three-dimensional cases,

$$\begin{aligned} \rho^{2D}(\mathbf{r}, \mathbf{r}'; \beta) &= \frac{1}{2\pi\sqrt{r r'}} \sum_{l=-\infty}^{+\infty} \rho_l(r, r'; \beta) e^{i l \Theta}, \\ \rho^{3D}(\mathbf{r}, \mathbf{r}'; \beta) &= \frac{1}{4\pi r r'} \sum_{l=0}^{+\infty} (2l+1) \rho_l(r, r'; \beta) P_l(\cos \Theta), \end{aligned} \quad (9)$$

where  $\Theta$  is the angle between  $\mathbf{r}$  and  $\mathbf{r}'$ . Each partial-wave component satisfies the 1D Bloch equation for a single particle in an external potential given by the interaction potential and also the convolution equation,

$$\rho_l(r, r'; \tau) = \int_0^\infty dr'' \rho_l(r, r''; \tau/2) \rho_l(r'', r'; \tau/2). \quad (10)$$

This is the basic equation of the *matrix-squaring method* which allows to calculate the function  $\rho_l$  at a given temperature  $1/\tau$  from the same function at a two times higher temperature. Squaring the density matrix  $k$  times results in a lowering of the temperature by a factor of  $2^k$ . Each squaring involves only a one-dimensional integration which, due to the Gaussian-like nature of the integrand in Eq. (10), can be performed quite accurately and efficiently by standard numerical procedures. To start the matrix-squaring iterations, Eq. (10), one needs a known accurate high-temperature form for the density matrix. A convenient choice is the semiclassical approximation

$$\rho_l(r, r'; \tau) = \rho_l^0(r, r'; \tau) \exp\left(-\frac{\tau}{|r - r'|} \int_r^{r'} V(x) dx\right), \quad (11)$$

where  $\rho_l^0(r, r'; \tau)$  is the partial-wave component of the free-particle density matrix.

Once the pair density matrix  $\rho_l(r, r'; \tau)$  is computed for the desired value of  $\tau$ , it is substituted into Eqs. (9-10), and a summation over partial waves readily yields the full relative density matrix.

#### B. Variational Approach for Density Matrices

As a second method for solving the off-diagonal Bloch equation we used a *variational perturbation expansion* developed by Feynman and Kleinert [34]. In this procedure the initial density matrix is presented in the form of a trial path integral which consists of a suitable superposition of local harmonic oscillator path integrals centered at arbitrary average positions  $\mathbf{x}_m$ , each with its own frequency squared  $\Omega^2(\mathbf{x}_m)$ . One starts from decomposing the action in the density matrix as

$$\rho(\mathbf{r}, \mathbf{r}'; \beta) = \int_{(\mathbf{r}, 0) \rightarrow (\mathbf{r}', \hbar\beta)} \mathcal{D}\mathbf{x} e^{-A[\mathbf{x}]/\hbar}, \quad (12)$$

$$A[\mathbf{x}] = A_{\Omega, \mathbf{x}_m}[\mathbf{x}] + A_{\text{int}}[\mathbf{x}], \quad (13)$$

with  $A_{\Omega, \mathbf{x}_m}[\mathbf{x}]$  being the action of a trial harmonic oscillator with the potential minimum located at  $\mathbf{x}_m$ , and  $\mathcal{D}$  being the functional integral over all trajectories. The interaction part

$$A_{int}[\mathbf{x}] = \int_0^{\hbar\beta} d\eta \left[ V[\mathbf{x}(\eta)] - \frac{1}{2}\mu \Omega^2 [\mathbf{x}(\eta) - \mathbf{x}_m]^2 \right], \quad (14)$$

is defined as the difference between the original potential  $V(\mathbf{x})$  and the displaced harmonic oscillator. The  $\Omega^2$  term in Eq. (14) compensates the contribution of  $A_{\Omega, \mathbf{x}_m}[\mathbf{x}]$  in Eq. (13). Now one can calculate the density matrix (12) by treating the interaction (14) as a perturbation, leading to a moment expansion

$$\begin{aligned} \rho(\mathbf{r}, \mathbf{r}') &= \rho_0^{\Omega, \mathbf{x}_m}(\mathbf{r}, \mathbf{r}') \left( 1 - \frac{1}{\hbar} \langle A_{int}[\mathbf{x}] \rangle_{\mathbf{r}, \mathbf{r}'}^{\Omega, \mathbf{x}_m} + \right. \\ &\left. + \frac{1}{2\hbar^2} \langle A_{int}^2[\mathbf{x}] \rangle_{\mathbf{r}, \mathbf{r}'}^{\Omega, \mathbf{x}_m} - \dots \right) = e^{-\tau W_N^{\Omega, \mathbf{x}_m}} \left( \frac{\mu}{2\pi\hbar^2\tau} \right)^{d/2}, \end{aligned} \quad (15)$$

with the definition

$$\begin{aligned} W_N^{\Omega, \mathbf{x}_m} &= \frac{d}{2\beta} \ln \frac{\sinh \hbar\beta\Omega}{\hbar\beta\Omega} + \frac{\mu\Omega}{2\hbar\beta \sinh \hbar\beta\Omega} \times \\ &\times [(\tilde{\mathbf{r}}^2 + \tilde{\mathbf{r}}'^2) \cosh \hbar\beta\Omega - 2\tilde{\mathbf{r}}\tilde{\mathbf{r}}'] - \\ &- \frac{1}{\beta} \sum_{n=1}^N \frac{(-1)^n}{n! \hbar^n} \langle A_{int}[\mathbf{x}] \rangle_{\mathbf{r}, \mathbf{r}'}^{\Omega, \mathbf{x}_m}, \end{aligned} \quad (16)$$

where  $d$  is the space dimensionality and  $N$  the order of the approximation. The function  $\rho_0^{\Omega, \mathbf{x}_m}(\mathbf{r}, \mathbf{r}')$  is the trial harmonic oscillator density matrix,  $\tilde{\mathbf{r}} = (\mathbf{r} - \mathbf{x}_m)$ ,  $\tilde{\mathbf{r}}' = (\mathbf{r}' - \mathbf{x}_m)$ , and the expectation value of the interaction action on the r.h.s. of Eq. (16) is given by

$$\begin{aligned} \langle A_{int}^n[\mathbf{x}] \rangle_{\mathbf{r}, \mathbf{r}'}^{\Omega, \mathbf{x}_m} &= \frac{1}{\rho_0^{\Omega, \mathbf{x}_m}(\mathbf{r}, \mathbf{r}')} \int_{\tilde{\mathbf{r}}, 0}^{\tilde{\mathbf{r}}', \hbar\beta} \mathcal{D}\tilde{\mathbf{x}} \prod_{l=1}^n \left\{ \int_0^{\hbar\beta} d\tau_l \times \right. \\ &\left. \times V_{int}[\tilde{\mathbf{x}}(\tau_l) + \mathbf{x}_m] e^{\{-\frac{1}{\hbar} A_{\Omega, \mathbf{x}_m}[\tilde{\mathbf{x}} + \mathbf{x}_m]\}} \right\}. \end{aligned} \quad (17)$$

The function  $W_N^{\Omega, \mathbf{x}_m}$  can be identified as an *effective quantum potential* which is to be optimized with respect to the variational parameters  $\{\Omega^2(\mathbf{r}, \mathbf{r}'), \mathbf{x}_m(\mathbf{r}, \mathbf{r}')\}$ . Note that, in the high temperature limit, this effective potential goes over to the original potential  $V(\mathbf{r})$ . The optimal parameter values are determined from the extremity conditions

$$\frac{\partial W_N^{\Omega, \mathbf{x}_m}(\mathbf{r}, \mathbf{r}')}{\partial \Omega^2} = 0, \quad \frac{\partial W_N^{\Omega, \mathbf{x}_m}(\mathbf{r}, \mathbf{r}')}{\partial \mathbf{x}_m} = 0. \quad (18)$$

The perturbation series (16) is rapidly converging, in most cases already in the first-order approximation  $W_1^{\Omega, \mathbf{x}_m}$  for the effective potential, and gives a reasonable estimate of the desired quantities. This will be illustrated in section IV by application of the *variational method* to an electron-proton pair and by comparison with the ‘exact’ solution from Sec. III A.

## IV. NUMERICAL RESULTS

In this section we consider application of effective quantum pair potentials to strongly correlated electron-proton pairs. After checking the accuracy of the effective potentials our main goal will be to extend them to situations beyond their original applicability, i.e. to  $\Gamma > 1$ . Before presenting the results for the quantum potentials, we briefly discuss their relevance for application in PIMC simulations of dense Coulomb systems, the corresponding numerical results will be given in Section IV E.

### A. Quantum pair potentials and Path integral Monte Carlo simulations

It is well known (see for example discussion in Chapter 12 of [34]) that the singularity of the attractive Coulomb potential causes difficulties in the euclidian path integral. If based on Feynman’s original path integral representation, a path consists of a *finite* number of straight pieces, each with a classical euclidian action, containing the singular Coulomb potential. However, in this case, the energy of the path can be lowered indefinitely by an almost stretched configuration which corresponds to a slowly moving particle sliding down to the  $-e^2/r$  abyss. This phenomenon is called *path collapse*.

One possibility to prevent this effect is to use a modified ‘regularized’ Coulomb potential which has a cutoff at  $r = 0$ . This procedure, however, is quite arbitrary, and the results are sensitive to the used cutoff parameters. Of course, in nature, these difficulties are prevented by quantum fluctuations which equip the path with a configurational entropy. The latter must be sufficiently singular to produce a regular free energy bounded from below. The inclusion of quantum fluctuations in the euclidean action of the Feynman path pieces smoothes the singular Coulomb potential, producing an effective potential that is finite at the origin, and the *path collapse* is avoided. This again shows the importance of effective potentials, specifically, in ‘quasiclassical’ simulations (classical Monte Carlo and molecular dynamics methods). Of great importance are potentials which have a closed analytical form. In this case for many thermodynamical quantities it is possible to obtain analytical solutions.

For simulations of correlated quantum many-body systems which are based on *first principles*, the initial many-body hamiltonian with the true singular Coulomb energy operator is to be considered and solved to find some effective many-body interaction potential. For this it is important that in the high-temperature limit the N-particle density matrix can be expanded in terms of 2-particle, 3-particle etc. contributions. If the temperature is sufficiently high then all contributions except the first one, taking into account two-particle correlations, can be omitted. As a result, the following approximation for the

N-particle density matrix holds

$$\rho(\mathbf{R}, \mathbf{R}'; \tau) \approx \prod_i^N \rho^{[1]}(\mathbf{r}_i, \mathbf{r}'_i; \tau) \times \prod_{j < k} \frac{\rho^{[2]}(\mathbf{r}_j, \mathbf{r}_k, \mathbf{r}'_j, \mathbf{r}'_k; \tau)}{\rho^{[1]}(\mathbf{r}_j, \mathbf{r}'_j; \tau) \rho^{[1]}(\mathbf{r}_k, \mathbf{r}'_k; \tau)} + O(\rho^{[3]}), \quad (19)$$

where  $\mathbf{R} = \{\mathbf{r}_1, \dots, \mathbf{r}_N\}$  specifies coordinates of all  $N$  particles,  $\rho^{[1]}$  ( $\rho^{[2]}$ ) is the single (two) particle density matrix. The above *pair* approximation is usually used in PIMC simulations [33]. The N-particle density matrix  $\rho(\beta)$  contains the complete information about the system with the observables given by

$$\langle \hat{O} \rangle = \frac{\text{Tr} [\hat{O} \hat{\rho}(\beta)]}{\text{Tr} [\hat{\rho}(\beta)]} = \frac{\int d\mathbf{R} \langle \mathbf{R} | \hat{O} \hat{\rho}(\beta) | \mathbf{R} \rangle}{\int d\mathbf{R} \langle \mathbf{R} | \hat{\rho}(\beta) | \mathbf{R} \rangle}. \quad (20)$$

Due to the exponential form, the N-particle density operator  $\hat{\rho}(\beta) = e^{-\beta \hat{H}}$  can be factorized (in analogy to the matrix squaring method above) as  $\hat{\rho}(\beta) = [\hat{\rho}(\tau)]^M$  with  $M = \beta/\tau$ . Consequently, the N-particle density operator  $\hat{\rho}(\beta)$  is expressed in terms of density operators at an  $M$  times higher temperature  $1/\tau = M \cdot k_B T$ . If  $M$  is chosen sufficiently large then one can apply the pair approximation (19). Thus, accurate results for the quantum pair potentials and, consequently, the pair density matrix, will allow to compute the density matrix of the whole  $N$ -particle system. Here we are not interested in the investigation of the accuracy of approximation (19) but concentrate on the two-body problem where Eq. (19) is exact.

It is clear that the observables (20) computed with the approximate pair-density matrix  $\rho^{[2]}$  contain an error of the order  $O(1/M^2)$ . Below, in Sec. IV E, we investigate the convergence, as a function of  $M$ , of main thermodynamic properties (total energy and e-p pair distribution) for an electron-proton pair using for the pair density matrix  $\rho^{[2]}$  results computed with the off-diagonal and the diagonal Kelbg potential.

### B. Diagonal and off-diagonal Kelbg potential results for the electron-proton pair density matrix

In Fig. 1 we show the angular dependence of the full off-diagonal two-particle density matrix calculated with the off-diagonal Kelbg potential – ODKP (3) and its diagonal approximation – DKP (4). The density matrix is shown at several temperature values ( $T = 1\,000\,000$ ,  $250\,000$  and  $62\,500$  K) and several angular distances ( $\phi = 0, \pi/2, \pi$ ) between the vectors  $\mathbf{r} \equiv \mathbf{r}_{ij}$ ,  $\mathbf{r}' \equiv \mathbf{r}'_{ij}$  (in each of the figures, the top curves correspond to the case of parallel vectors,  $\phi = 0$ , the lowest curves to antiparallel vectors,  $\phi = \pi$ ). Also, for reference, we give the off-diagonal density matrix obtained from the ‘exact’ solution of the Bloch equation, cf. Sec. III A. At high

temperatures,  $T \geq 250\,000$  K, the Kelbg density matrix does not exhibit large deviations from the exact result. At  $T = 1\,000\,000$  K, the ODKP density matrix practically coincides with the exact solution, whereas the DKP approximation shows small deviations. In these cases the perturbation expansion applies,  $\Gamma \sim 0.15$ , see left column of Fig. 1. With decreasing temperature, the deviations from the exact results grow, see middle column. To better understand the details of the deviations, we magnified them by including also results for  $T = 62\,500$  K, which is far beyond the scope of the perturbation theory,  $T \approx 0.4 Ry/k_B$ , i.e.  $\Gamma \approx 2.5$ . Here we observe that, at the origin, the density matrix of the Kelbg potential is 3 times less than the exact one. The largest errors were found for the DKP, in particular, in the case when the vectors  $\mathbf{r}, \mathbf{r}'$  have the opposite direction ( $\phi = \pi$ ).

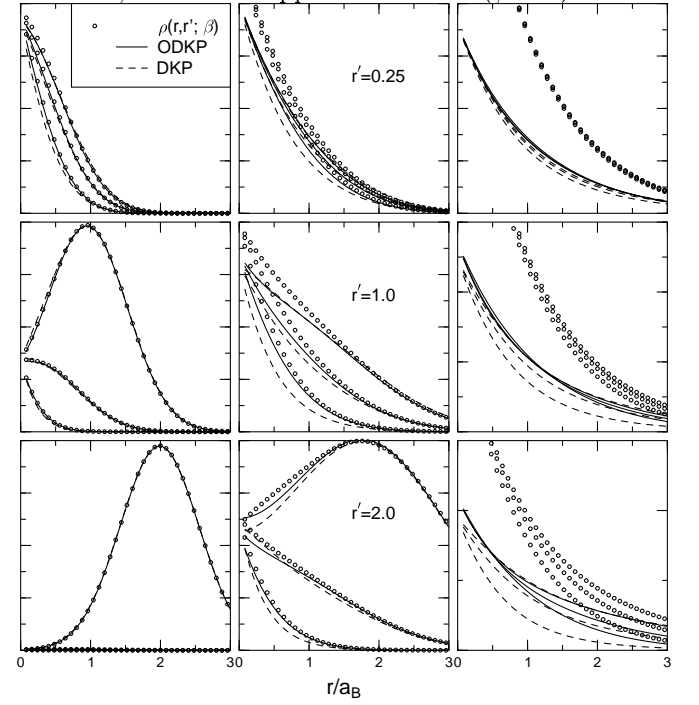


Figure 1: The ‘exact’ off-diagonal density matrix  $\rho(r, r'; \phi)$  for an electron-proton pair vs. the density matrix calculated with the diagonal (DKP) and off-diagonal (ODKP) Kelbg potentials. In all figures, results for three angular values are given  $\phi = 0$  (upper curves),  $\phi = \pi/2$  (middle) and  $\phi = \pi$  (lower curves). The proton is located at the origin, and the vector  $\mathbf{r}'$  (initial electron position) is fixed,  $|\mathbf{r}'| = 0.25; 1.0; 2.0$ . The vector  $\mathbf{r}$  (final electron position) is varied,  $\phi$  is the angle between the vectors  $\mathbf{r}$  and  $\mathbf{r}'$ .

The behavior of the full density matrix can be understood from the following considerations. The density matrix results from contributions of kinetic and potential energy operators, cf. Eq. (1). At small distances ( $r' = 0.25$ ) the Coulomb attraction between an electron and a proton dominates and, therefore, the density matrix shows an exponential decay. At the largest distance ( $r' = 2.0$ ) kinetic and potential energy are of the same order and a Gaussian-like free particle density matrix emerges, as can be clearly seen in the bottom left part of Fig. 1.

From this first comparison we can conclude that both, the DKP and the ODKP, show satisfactory agreement with the exact result in the cases where perturbation theory applies,  $T \gtrsim 2$  Ry. At lower temperatures there is only qualitative agreement. The strongest deviations arise for small interparticle distances  $\{\mathbf{r}, \mathbf{r}'\}$ , and this, as will be shown below, results from the incorrect height of the Kelbg potential at zero distance  $r = 0$ .

### C. Effective electron-proton and electron-electron quantum pair potentials

In Fig. 2 we compare the effective electron-proton potentials obtained using various methods. Here the DKP (4) and the variational potential (16) are plotted vs. the quantum pair potential which follows from the 'exact' two-body diagonal matrix element by the definition

$$\rho(r, r; \beta) \equiv \frac{1}{\lambda_\beta^d} e^{-\beta U_p(r; \beta)} \Rightarrow \\ \Rightarrow U_p = -\frac{1}{\beta} \ln [\lambda_\beta^d \rho(r, r; \beta)]. \quad (21)$$

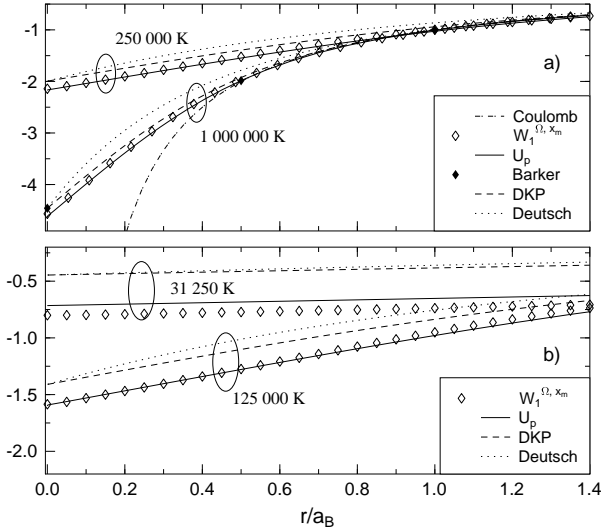


Figure 2: Diagonal effective pair potentials (in units of Ha) for several cases: the DKP  $\Phi(\mathbf{r}, \mathbf{r}; \beta)$  (4), variational potential  $W_1^{\Omega, \chi_m}$  (16), pair potential  $U_p$  (21) corresponding to the 'exact' density matrix, numerical results of Barker [32], the Deutsch potential [21] and the pure Coulomb potential. Each potential is given at three temperature values: (a) 250 000 and 1 000 000 K, (b)  $T = 31\,250$  and 125 000 K.

Calculation results from a direct eigenfunction summation by Barker [32] are also included. First, we see that the accuracy of the DKP is satisfactory for temperature  $T = 1\,000\,000$  K and above. At lower temperatures ( $T = 31\,250, 125\,000, 250\,000$  K) a systematic offset appears at the origin,  $r = 0$ . This offset increases with

lowering of the temperature and leads to increasing deviations of the DKP density matrix from the exact one for temperatures below 1 Ry (this is also confirmed by Fig. 1, cf. column for  $T = 62\,500$  K). Interestingly, we can note, that these deviations are rather trivial: in all cases the DKP goes almost parallel to the 'exact' potential  $U_p$ , in particular, it has the same  $r$ -derivative at  $r = 0$ , see [36]. This suggests that a simple correction of the DKP value at  $r = 0$  may significantly improve the accuracy, as will be confirmed below in Sec. IV D.

As far as other quantum pair potentials are concerned, their deviations from the exact result is larger than for the Kelbg potential. As a typical example, we show in Fig. 2 also results for the Deutsch potential. As one can see, the Deutsch potential has the same value at  $r = 0$  as the Kelbg potential but a different spatial derivative  $U'_r$  at the origin, which leads to deviations for  $r < a_B$ . As can be seen from the figure, these deviations decrease with lowering the temperature.

Interestingly, the variational potential (Sec. IIIB) is more accurate than the DKP and reproduces the 'exact' effective pair potential for temperatures  $T \gtrsim 50\,000$  K sufficiently well. The key point in its behavior is that the *variational perturbation theory* [34] transforms the perturbation expansion in  $\Gamma$  (which doesn't converge for  $\Gamma \gtrsim 1$ ) into another expansion, Eq. (15), which does not have this restriction. The convergence of Eq. (15) even extends to very strong coupling and has recently been successfully applied in field theory [35].

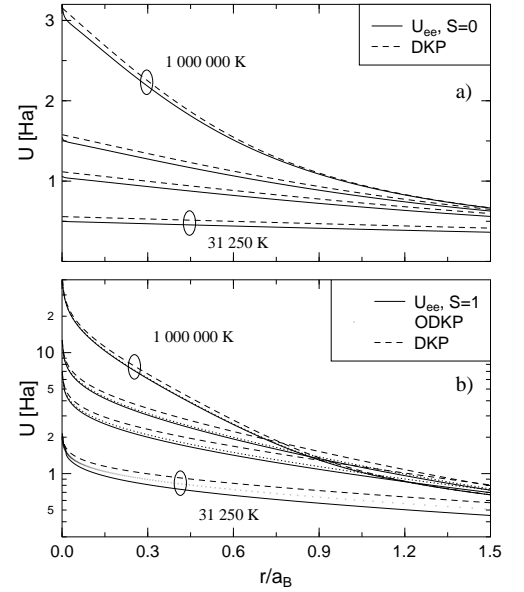


Figure 3: Diagonal effective quantum pair potentials (in units of Ha) for electron-electron interaction. *Top*: antiparallel spins ( $S = 0$ ),  $U_{ee}^{\downarrow\downarrow}$  - 'exact' pair potential versus DKP. *Bottom*: parallel spins ( $S = 1$ ),  $U_{ee}^{\uparrow\uparrow}$  - 'exact' pair potential, ODKP - using the anti-symmetrical density matrix (23), DKP - using Eq. (24). Each potential is given at four temperature values:  $T = 31\,250, 125\,000, 250\,000$  and 1 000 000 K.

Next, in Fig. 3, we compare the effective potentials

for electron-electron interaction considering two possible cases of spin projections (triplet and singlet states). Top (bottom) figure shows the case when electron spins are antiparallel (parallel). It can be seen that spin effects play an important role, being especially important at small distances,  $r \leq a_B$ . The value of  $U_{ee}^{\uparrow\uparrow}(0)$  is infinite, reflecting the Pauli principle, whereas  $U_{ee}^{\uparrow\downarrow}(0)$  remains finite. Even at high temperatures  $U_{ee}^{\uparrow\uparrow}$  differs significantly from  $U_{ee}^{\uparrow\downarrow}$ . At low temperatures, it appears as if spin effects become relatively less important, but this is not entirely true. Most macroscopic properties depend on  $(e^{-\beta U})$ , and with decreasing temperature the product  $\beta U$  is an increasing function, this means that the importance of the small distance region also increases.

In Fig. 3 we also compare the effective potentials obtained in the Kelbg approximation. First, for the case when the electrons are distinguishable particles, the potential  $U_{ee}^{\uparrow\downarrow}$  coincides with the DKP (4). One can note that the e-e DKP is significantly closer to the ‘exact’ pair potential than the e-p DKP, cf. Fig. 2, which is due to the contribution from bound states in the case of the attractive interaction.

For parallel spins, the coordinate part of the two-electron wave function (or the corresponding pair density matrix) must be anti-symmetric. This means that now the effective quantum potential has to be defined in the following way

$$e^{-\beta U_{ee}^{\uparrow\uparrow}} = \rho_A(\mathbf{r}_i, \mathbf{r}_j, \mathbf{r}_i, \mathbf{r}_j; \beta) = \rho_{cm}(\mathbf{R}, \mathbf{R}) \{ \rho(\mathbf{r}, \mathbf{r}) - \rho(\mathbf{r}, -\mathbf{r}) \}, \quad (22)$$

where the two-particle density matrix is factorized into density matrices depending on the center-of-mass and relative coordinates, respectively. Taking into account that the free particle density matrix  $\rho_{cm}(\mathbf{R}, \mathbf{R}) = 1$  and using, for  $\rho(\mathbf{r}, \mathbf{r})$ , the result of Eq. (2), the effective potential for electrons with parallel spins reads

$$U_{ee}^{\uparrow\uparrow} = -\frac{1}{\beta} \ln \left( e^{-\beta \Phi^{ij}(\mathbf{r}, \mathbf{r})} - e^{-\frac{4\mu_{ij}}{2\hbar^2 \beta} r^2} e^{-\beta \Phi^{ij}(\mathbf{r}, -\mathbf{r})} \right). \quad (23)$$

Here, for the off-diagonal density matrix, we use the combination of Eqs. (2) and (3). The contribution to exchange arises not only from the kinetic energy part of the density matrix but also from the non-diagonal potential,  $\Phi^{ij}(\mathbf{r}, -\mathbf{r})$ , calculated with (3). Finally, if the off-diagonal potential term  $\Phi^{ij}(\mathbf{r}, -\mathbf{r})$  is approximated by its diagonal matrix elements, i.e. by the DKP, the above expression reduces to

$$U_{ee}^{\uparrow\uparrow} = \Phi^{ij}(\mathbf{r}, \mathbf{r}) - \frac{1}{\beta} \ln \left\{ 1 - e^{-\frac{4\mu_{ij}}{2\hbar^2 \beta} r^2} \right\}. \quad (24)$$

At  $r \rightarrow 0$ , this potential shows a logarithmic divergency.

In Fig. 3 the results for these two cases – the antisymmetric ODKP and DKP are shown. One can note that the diagonal approximation (24) is less accurate than the ODKP (23) at all temperatures. At  $T = 1\,000\,000$  K the

effective potential (23) practically coincides with the potential  $U_{ee}$  obtained from the ‘exact’ two-particle density matrix.

In summary, both the DKP and the ODKP show good agreement with the ‘exact’ result in a wide temperature range corresponding to the validity of the weak coupling approximation. Moreover, at lower temperature, the most deviations appear to be correctable with a simple shift in the values at  $r \lesssim a_B$ . We now use this idea to construct improved Kelbg potentials which are accurate also beyond the weak coupling limit.

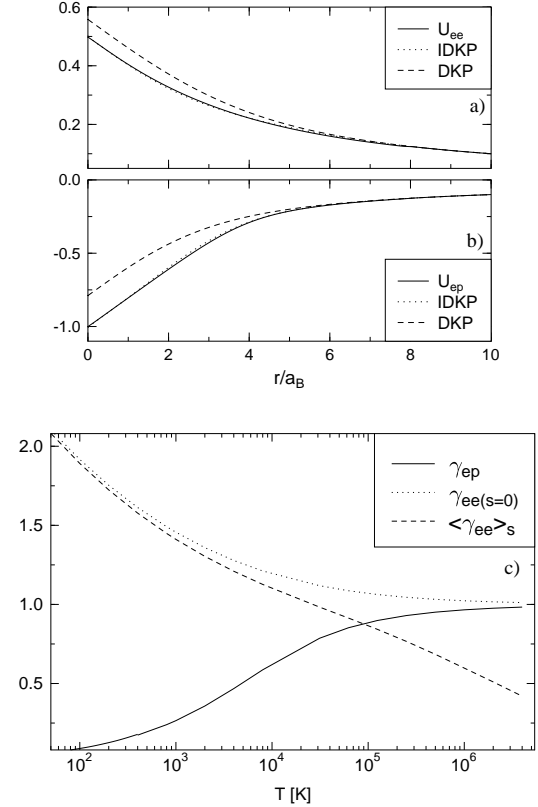


Figure 4: (a): Electron-electron and (b): electron-proton diagonal Kelbg potential (DKP), Eq. (4) and improved diagonal Kelbg potential (IDKP), Eq. (25), vs. ‘exact’ pair potential  $U_{ee}(U_{ep})$ , Eq. (21), at  $T = 31\,250$  K. (c): fit parameter  $\gamma_{ij}$  as a function of temperature for electron-proton interaction,  $\gamma_{ep}$ , and electron-electron interactions with antiparallel spins,  $\gamma_{ee}(s=0)$ . Also shown is the fit parameter for the spin-averaged potential,  $\langle \gamma_{ee} \rangle_s$ .

#### D. Improved effective potentials

Improved Kelbg potentials were considered in [37] and in [42], where it was suggested that, for the free charges, the real interactions have the same functional form as the

Kelbg potential with an additional free parameter  $\gamma_{ij}$

$$\begin{aligned} \Phi(r_{ij}, \beta) &= \\ &= \frac{e_i e_j}{r_{ij}} \left[ 1 - e^{-\frac{r_{ij}^2}{\lambda_{ij}^2}} + \sqrt{\pi} \frac{r_{ij}}{\lambda_{ij} \gamma_{ij}} \left( 1 - \operatorname{erf}(\gamma_{ij} \frac{r_{ij}}{\lambda_{ij}}) \right) \right]. \end{aligned} \quad (25)$$

This modified potential has a new degree of freedom in its value at  $r = 0$  which is governed by  $\gamma_{ij}$ ,

$$\Phi(\mathbf{r}_{ij} = 0, \beta) = \frac{e_i e_j \sqrt{\pi}}{\lambda_{ij} \gamma_{ij}}. \quad (26)$$

At the same time, Eq. (25) preserves the correct first derivative at the origin,  $\Phi(0, \beta)'_r = -\frac{e_i e_j}{\lambda_{ij}^2}$ , of the original Kelbg potential (4).

For the case  $\gamma_{ij} = 1$ , Eq. (25) coincides with Eq. (4). The single parameter  $\gamma_{ij}$  allows us to correct the height of the DKP at  $r = 0$  in such a way that the improved Kelbg potential has a good quantitative agreement with the ‘exact’ pair potential  $U_p$  in a very large range of temperatures. To obtain the correct zero-point value of the DKP we allow for a temperature dependence of the fit parameter,  $\gamma_{ij} = \gamma_{ij}(T)$ . In Fig. 4 we compare the DKP, improved DKP and pair potential  $U$ . One can see that with the additional parameter  $\gamma_{ij}$  the improved DKP practically coincides with the ‘exact’ potential. We show results for electron-proton and electron-electron interaction for antiparallel spins.

The temperature dependence of  $\gamma_{ij}$  was obtained by fitting the values of  $\Phi(\mathbf{r}_{ij}, \beta)$  to those of the exact potential,  $U_p$  (21), at  $r = 0$ . The results of this fitting procedure are shown at the bottom of Fig. 4. For comparison, we also made analytical calculations using the method of Slater sums [42]. Both methods give identical results.

For example, the binary Slater sum of two electrons  $i$  and  $j$  at zero distance is given by (symmetry effects are also included)

$$S_{ee}^{\uparrow\downarrow}(r_{ee} = 0) = 4\sqrt{\pi}\xi_{ee}J_1(\xi_{ee}), \quad (27)$$

$$\langle S_{ee}(r_{ee} = 0) \rangle_s = 2\sqrt{\pi}\xi_{ee}J_1(\xi_{ee}), \quad (28)$$

$$J_1(\xi_{ij}) = \int_0^\infty e^{-x^2} \frac{x dx}{1 - \exp(-\frac{\pi\xi_{ij}}{x})}, \quad (29)$$

where the interaction parameter  $\xi_{ij} = e_i e_j \beta / \lambda_{ij}$ . In the second expression the Slater sum includes the average over two possible spin projections.

The electron-proton Slater sum at zero distance can be written as

$$S_{ep}(r_{ep} = 0) = 4\sqrt{\pi}\xi_{ep}J_1(\xi_{ep}) + \sqrt{\pi}\xi_{ep}^3 Z_3(\xi_{ep}), \quad (30)$$

$$Z_n(\xi) = \sum_{y=1}^\infty y^{-n} e^{\xi^2/4y^2}. \quad (31)$$

Using the definition of the effective potential

$$e^{-\beta U_{ij}} \equiv S_{ij} \quad (32)$$

and Eq. (25), the fit parameter  $\gamma_{ij}$  at zero interparticle distance can be defined as

$$\gamma_{ij}(r_{ij} = 0) = -\frac{\sqrt{\pi}}{\lambda_{ij}} \frac{e_i e_j \beta}{\ln[S_{ij}(r_{ij} = 0)]}. \quad (33)$$

We found that the temperature dependence of  $\gamma_{ij}$  can be well described by the following Padé approximations which are useful for practical applications:

$$\gamma_{ep}(T) = \frac{x_1 + b_{ep} x_1^2}{1 + a_{ep} x_1 + b_{ep} x_1^2}, \quad (34)$$

$$\gamma_{ee}^{\uparrow\downarrow}(T)_{s=0} = \frac{\gamma_{ee}^{\uparrow\downarrow}(T \rightarrow 0) + b_{ee} x_1^2}{1 + a_{ee} x_1 + b_{ee} x_1^2}, \quad (35)$$

where  $x_1 = \sqrt{8\pi k_B T / \text{Ha}}$  (one Hartree is  $\text{Ha} = 2\text{Ry} = 315\,775\text{ K}$ ),  $b_{ep} = 1$ ,  $b_{ee} = 1$ ,  $a_{ep} = 1.10(1)$ ,  $a_{ee} = 0.180(2)$ . The limit  $\gamma_{ee}(T \rightarrow 0)$  has been found from Eq. (33) by evaluating the zero temperature limit of Eq. (27):

$$\gamma_{ee}^{\uparrow\downarrow}(T \rightarrow 0) \approx -\frac{2}{\sqrt{\pi}} \tilde{x}^3 \frac{1}{\ln\{8\tilde{x}^4/\sqrt{\pi}\} - 3\tilde{x}^2}, \quad (36)$$

with  $\tilde{x} = (|\pi \xi_{ee}|/2)^{\frac{1}{3}}$ .

The physical content of Fig. 4 is the following: in the limit of high temperatures, both correction parameters,  $\gamma_{ep}$  and  $\gamma_{ee}(S = 0)$ , approach 1, i.e.  $\tilde{\Phi}_{ij} \rightarrow \Phi_{ij}$ , which means that the height of the potential at  $r_{ij} = 0$  is determined by the De Broglie wavelength of *free* particles,  $\lambda_{ij}$  [44]. For temperatures below one Rydberg  $\gamma_{ij}$ , start to deviate from 1. The quantum extension of particles is becoming influenced by interaction effects and is now of the order of  $\tilde{\lambda}_{ij} = \lambda_{ij} \gamma_{ij}$ , instead of thermal wavelength  $\lambda_{ij}$ .

Consider first the e-p interaction. Here, obviously, for  $T \rightarrow 0$ , the correct potential value is given by the ground state energy of a hydrogen atom, i.e.  $\tilde{\Phi}_{ep}(0) \rightarrow -e^2/2a_B$ . This leads to  $\gamma_{ep} \rightarrow 2a_B/\lambda_{ep}$ , i.e. the effective quantum extension of the electron is given by the Bohr radius. For a pair of electrons, on the other hand, if the temperature is lowered, the Coulomb repulsion leads to a growth of the effective quantum wavelength above the De Broglie value, as can be clearly seen in Fig. 4. Thus the results for  $\gamma_{ij}$  are of physical value by themselves: multiplied with the DeBroglie wavelength, they reflect the correct ‘quantum size’ of an electron when interacting with a proton or a second electron, respectively.

Due to the corrected value of the electron ‘size’, the improved Kelbg potentials (25) are much closer to the ‘exact’ result for the quantum pair potential, Eq. (21). Most importantly, the potentials (25) are *not limited to weak coupling* as is the original Kelbg potential and are, therefore, of high value for both analytical and computational studies of quantum plasmas.

Finally, we underline that we correctly account for the possible spin projections of the electrons. Alternatively, one can derive a different quantum pair potential which



is averaged over the spin projections. The corresponding averaged correction factor is also included in Fig. 4, cf. the dashed line. While this factor is also obtained from the fit to the exact (spin averaged) pair density matrix and thus correctly reproduces the thermodynamic properties, the spin-resolved approximation is essentially superior: it allows for a refined modeling and simulation of quantum plasmas. In particular, it allows for the inclusion of spin-dependent effects which is important, in particular, in the presence of a magnetic field.

### E. Application of the DKP and ODKP to PIMC simulations

We now analyze the application of effective quantum pair potentials in path integral Monte Carlo simulations. We consider a hydrogen atom in a box with periodic boundary conditions (box size,  $L = 20 a_B$ ) at several temperatures,  $T = 31\,250 - 62\,500$  K, when the hydrogen atom can ionize into free particles, as well as for the case  $T < 10\,000$  K, when there is essentially only the contribution from the atomic ground state. First, in Fig. 5 we show the e-p pair distribution functions (normalized to the volume  $dV = 4\pi r^2 dr$ ).

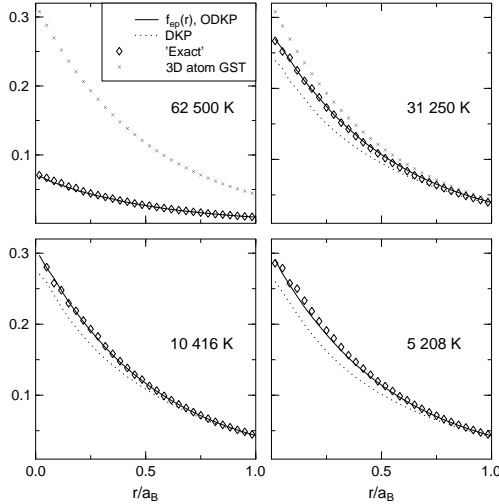


Figure 5: Proton-electron pair correlation functions from PIMC simulations which used the ‘exact’ pair density matrix (diamonds), the DKP (dots) and the ODKP (full line). Temperature values are as indicated in the figure parts:  $T = 5\,208, 10\,416, 31\,250$  and  $62\,500$  K. For comparison, ‘3D GST’ – denotes the pair correlation function corresponding to the ground state of a hydrogen atom.

For temperatures  $T = 5\,208$  K and  $10\,416$  K the hydrogen atom does not decay into free particles during the duration of a typical simulation run ( $\sim 10^6$  Monte Carlo steps). In the figures, the ‘exact’ pair correlation function is compared with the one obtained with the off-diagonal and diagonal Kelbg potentials, respectively (the number of factorization factors for the density matrix was

chosen to be  $M = 400$ ). We found that the best accuracy is achieved for the off-diagonal Kelbg potential and  $M \gtrsim 200$ , in this case the ODKP pair correlation function is very close to the exact one.

At elevated temperatures,  $T = 31\,250$  K and  $62\,500$  K, ionization of the hydrogen atom occurs, but due to the periodic boundary conditions, the free particles cannot go to infinity but, when reaching the boundary, are returned back in the simulation box and have a finite probability for a formation of a bound state again. Thus, this simulation captures the region of partial ionization. As the temperature is increased the ionization probability also increases, leading to a significant drop in the height of the proton-electron pair distribution function at the origin compared to the ground state probability function  $\Psi_0^2(r)$ , (see Fig. 5, plots for  $T=31\,250$  K and  $T=62\,500$  K).

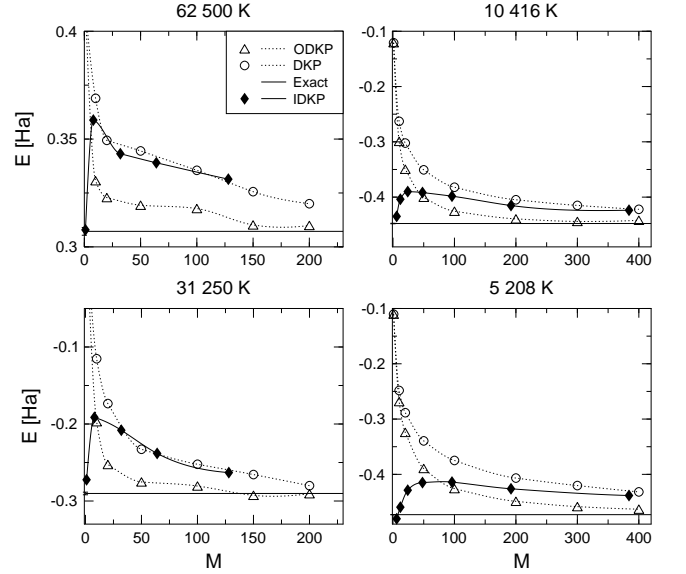


Figure 6: PIMC results for the internal energy of the proton-electron pair using ‘exact’ pair density matrix, DKP, ODKP and Improved Kelbg potential vs. different number of factorization factors  $M$ .

In Fig. 6 we analyze the convergence of the internal energy in PIMC simulations with varying number of high-temperature factors  $M$ . In particular, we compare independent simulations which used the diagonal and off-diagonal Kelbg density matrices, respectively. The ‘exact’ energy value for the considered temperatures is given by the solid line and is obtained from PIMC simulations using the ‘exact’ pair density matrix, cf. Sec. III A). The internal energy was obtained using the thermodynamic estimator,  $\langle E \rangle = -\frac{\partial}{\partial \beta} \ln Z$ , where  $Z$  is the partition function. Comparing the *diagonal* and *off-diagonal* cases one can note that the ODKP density matrix shows much better and faster convergence to the exact energy value. A simple estimate shows that the relative error of the total energy, in the diagonal approximation, depends on factorization number  $M$  as  $\delta E/E \approx \gamma \tau^2$ ,  $\tau = \beta/M$ . In contrast, using the off-diagonal potential, the error con-

verges much faster,  $\delta E/E \approx \gamma\tau^3$ .

This fact is illustrated in Fig. 7 where the logarithm of the relative error,  $\log(\delta E/E)$ , is shown as a function of the inverse of the temperature used in the high-temperature factors,  $1/\tau$ . In this figure we compare the behavior of the error for the same set of temperatures as in Fig. 6. In Fig. 6 we also add simulation results using *improved diagonal* Kelbg potential (solid line). Its accuracy is better than that of the ODKP at low temperatures (small values of  $M$ ) but at high temperatures both are comparable.

The main conclusion that can be drawn from the presented PIMC results is that, at equal number of factorization factors  $M$ , simulations with the off-diagonal Kelbg potential are significantly more accurate in reproducing the ‘exact’ thermodynamic results of a hydrogen atom. Besides, the full off-diagonal density matrix contains valuable information about the spatial electron distribution around the proton, which is lost in the end-point approximation. Further, we expect that the best results will be obtained using an *improved off-diagonal* Kelbg potential, which has the correct zero-point value and contains the complete angular dependence of the pair density matrix which, however, is beyond the scope of the present paper.

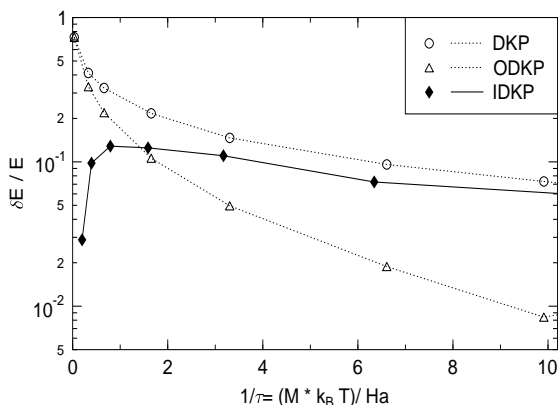


Figure 7: Relative error in the internal energy of the proton-electron pair from PIMC simulations with diagonal, off-diagonal Kelbg potential vs. temperature argument in the two-particle density matrix  $1/\tau$ .

## V. MOLECULAR DYNAMICS SIMULATIONS

In this section, we apply the improved Kelbg potentials in classical molecular dynamics simulations of dense hydrogen. Classical MD simulations of dense plasmas have been performed by many authors before where the divergency at zero distance leading, in particular, to the classical collapse of an electron into a proton, is usually avoided by some cutoff or ‘regularization’ of the Coulomb

potential at small distances. Using in this paper, effective quantum pair potentials obtained from the exact solutions of the Bloch equations, we expect to be on well founded grounds regarding the correct pair interactions at short distances. This should not only prevent any collapse but also correctly reproduce the formation of hydrogen atoms and thus allow us to obtain essentially improved MD simulation results. On the other hand, this is not a trivial question, since these potentials are derived from pure equilibrium considerations, and there is no ad-hoc proof that they will necessarily be accurate for the description of dynamical behavior as well, in particular under strong nonequilibrium conditions. We, therefore, concentrate in the present analysis on correlated partially ionized hydrogen in *thermodynamic equilibrium*. The results obtained below confirm that, indeed (at least in equilibrium), the quantum pair potentials are well suited for use in the interparticle force terms in classical MD.

Classical MD simulations incorporate all interparticle collision processes and are thus not restricted with respect to the coupling parameter  $\Gamma$  in a classical system. With the use of effective quantum pair potentials, we expect, in addition, to capture dominant features of the quantum nature of microparticles, such as quantum diffraction and spin effects. Thus, these simulations could be called ‘semiclassical’ MD. Having access not only to improved electron-ion potentials but also to spin-dependent electron-electron potentials, allows us to consider also spin effects by simulating electrons with different spin projections as two independent particle species. No spin-flip processes, as they would be expected e.g. in strong magnetic fields are considered, but our model should be capable to describe related phenomena as well. In this paper we focus on static properties, such as internal energy, and radial distribution functions. Investigation of dynamical properties and of spin density fluctuation is the aim of a forthcoming paper.

We consider a dense, degenerate hydrogen plasma at two densities corresponding to the Brueckner parameter  $r_s = \bar{r}/a_B = 4$  and  $r_s = 6$  and temperatures  $T = 31\,250, 50\,000, 62\,500, 125\,000$  and  $166\,670$  K. These parameter values correspond, respectively, to  $\Gamma = 2.53, 1.58, 1.26, 0.63$  and  $0.47$ , for  $r_s = 4$ , and  $1.68, 1.05, 0.84, 0.42, 0.32$ , for  $r_s = 6$ .

The simulation box of our system, with the length  $L = [n/(N_p + N_e^\uparrow + N_e^\downarrow)]^{1/3}$ , contains  $N_p = 200$  protons,  $N_e^\uparrow = 100$  electrons with spin up and an equal number of electrons,  $N_e^\downarrow = 100$ , with spin down. We keep the condition of the electro neutrality by taking  $N_p = N_e^\downarrow + N_e^\uparrow$ . Details of the used numerical algorithm can be found in Ref. [17].

Since MD, in contrast to PIMC, involves only diagonal interaction potentials, we choose the following expressions: for the interaction between electrons and protons, protons and protons and electrons with opposite spin, we use the improved Kelbg potential, Eq. (25), with the fit parameters given by Eqs. (34) and (35), respectively. The interaction between electrons with the same

spin projection is described by the diagonal antisymmetric potential, Eq. (24). Further, to properly account for the long range-character of the potentials, we used the standard Ewald procedure as in Ref. [17] whereas, in contrast to the rather involved expressions given there for a one-component plasma, here we could restrict the potential energy sum only by the proper sum in *real space* (we do not reproduce these lengthy expressions here, but mention that the value of the parameter  $\alpha$  defined in Ref. [17] was chosen to be  $\alpha = 5.6/L$ ) and taking 5 vectors in every direction in *the reciprocal space*. This gives some computational-cost advantage in computation of the forces compared to Ref. [17].

In Fig. 8, we plot the internal energy per atom as a function of temperature for two densities and compare it to the path integral Monte Carlo results of Militzer [43]. One can note, that for high temperatures the energies of MD and PIMC simulations coincide very well and lie within the limits of the statistical errors. This is an important test for the simulation, and this agreement was expected due to the asymptotic character of the Kelbg potential as a rigorous weak coupling result. Moreover, we observe practically full agreement between MD and PIMC results to temperature as low as approximately 50,000K, corresponding to a coupling parameter  $\Gamma = 3$ . This is a remarkable extension of ‘semiclassical’ molecular dynamics into the regime of moderate coupling and moderate degeneracy.

Naturally, below a critical temperature of about 50,000K deviations from PIMC results start to grow rapidly – the MD results for the energy are becoming very low. It is very interesting to analyze the reasons for these deviations, as this may suggest directions for further improvements. It turns out that the reason for these deviations is not a failure of the used quantum pair potentials. Thus the only source for the deviations in the full simulation can be many-particle effects beyond the two-particle level.

To verify this hypothesis we performed a careful inspection of the microscopic particle configurations in the simulation box. At high temperatures, the particle trajectories are those of a fully ionized classical plasma. At temperatures below on Ry, we observe an increasing number of electrons undergoing strong deflections on protons and eventually performing quasibound trajectories. Most of these electrons remain “bound” only for a few classical orbits and then leave the proton again. Averaged over a long time our simulations are able to reveal the degree of ionization of the plasma. At the same time we observe occasional events of three and more particles being at short distances for the duration of one or more orbits, reflecting the appearance of hydrogen molecules  $H_2$ , molecular ions  $H_2^+$  etc.

If the temperature is lowered below approximately  $T = 50,000K$ , we observe a strong increase of molecule formation and even a aggregation of many molecules into clusters with an interparticle distance close to one  $a_B$ . This turns out to be the reason for the observed very

low energy because the attractive Coulomb interaction contributions are becoming dominant in the total energy. Of course, this behavior is not surprising: while all pair interaction processes are modeled correctly even at low temperature (which is assured by the fit parameters in the improved Kelbg potentials), as soon as three or more particles are being closely together, three-particle and higher order correlations are becoming increasingly strong (they, in particular, account for the formation of the larger bound state complexes described above). However, it was just the approximation used in the derivation of the quantum potentials that three-particle and higher correlations can be neglected which was the basis for the use of pair potentials in modeling the whole  $N$ -particle system. While molecular dynamics, of course, includes any level of correlations, the use of the present potentials means that *quantum corrections to three-body (and higher order) interactions* are not adequately captured. Therefore, it is no surprise that this approximation breaks down at sufficiently low temperature, and this break down occurs around the temperature corresponding to the binding energy of hydrogen molecules. From this we can conclude that molecule formation sets the limit of the applicability of the present semiclassical MD simulations.

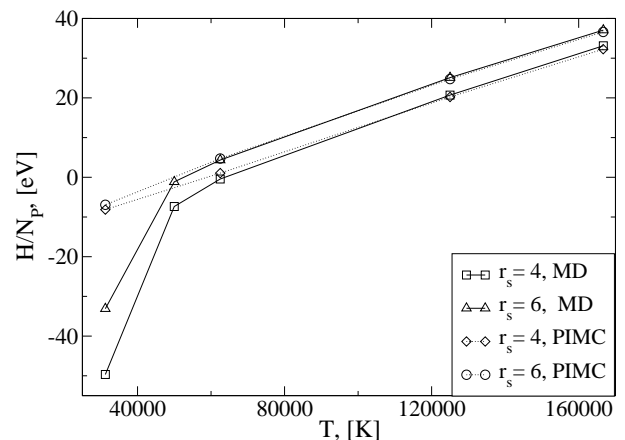


Figure 8: Semiclassical MD results (full lines) for the internal energy per hydrogen atom at densities  $r_s = 4, 6$  versus temperature. The results of restricted PIMC simulations by Militzer [43] are shown for comparison (dashed lines). Symbols indicate the five temperatures for which MD simulations have been performed:  $T = 31\,250, 50\,000, 62\,500, 125\,000$  and  $166\,670$  K (solid lines). The pair approximation breaks down around 50,000K, at the molecule binding energy.

Let us now turn to a more detailed analysis of the spatial configuration of the particles in the MD simulations.

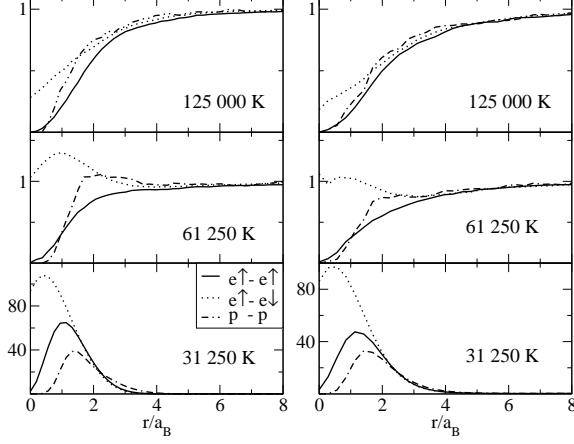


Figure 9: Electron-electron and proton-proton radial pair distribution functions for a correlated hydrogen plasma with  $r_s = 4$  (left row) and  $r_s = 6$  (right row) for  $T = 125\,000$ ,  $61\,250$  and  $31\,250$  K (from top to bottom).

In Fig. 9 the radial pair distributions between all particle species with the same charge are plotted at two densities. Consider first the case of  $T = 125\,000$  K (upper panel). For both densities, all functions look qualitatively the same, showing a depletion at zero distance due to Coulomb repulsion. Besides, there are differences which arise from the spin properties. Electrons with same spin show a slightly broader “Coulomb hole” around  $r = 0$  than the protons, because the Pauli principle yields an additional repulsion of the electrons (this effect is much weaker for two protons due to their much smaller De-Broglie wavelength). This trend is reversed at lower temperature, see middle panel, which is due to the formation of hydrogen atoms, see also Fig. 11 below. In this case, electrons (their trajectories) are “spread out” around the protons giving rise to an increased probability of close encounters of two electrons in different atoms compared to two protons.

Now, let us compare electrons with parallel vs. electrons with antiparallel spins. In all cases, we observe a significantly increased probability to find two electrons with opposite spin and small distances below one Bohr radius which is due to the missing Pauli repulsion in this case. This trend increases with lowering of temperature due to increasing quantum effects and thus convincingly confirms that spin effects are correctly reproduced in our MD simulations.

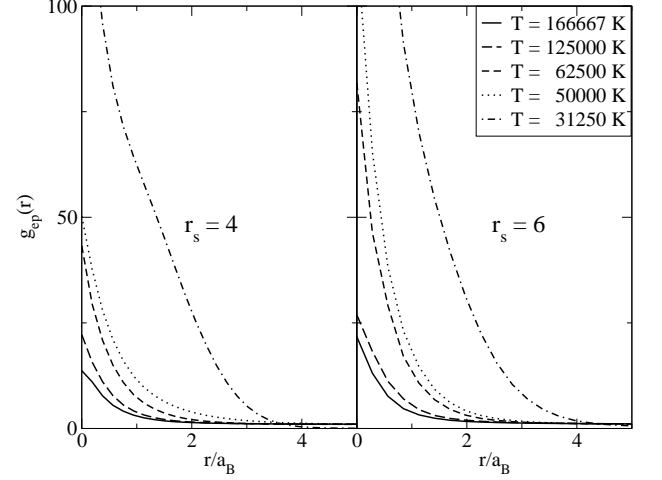


Figure 10: Electron-proton radial pair distribution functions at  $r_s = 4$  (left figure) and  $r_s = 6$  (right figure) and five temperatures:  $T = 166\,667$ ,  $125\,000$ ,  $62\,500$  and  $31\,250$  K.

Before analyzing the lowest temperature in Fig. 9 let us consider the electron-proton pair distributions which are shown in Fig. 10. With lowering of temperature, we observe a strong increase of the probability to find an electron close to a proton. In contrast to the classical case of a collapse (see above), here this probability is finite. Multiplying these functions by  $r^2$  gives essentially the radial probability which is plotted in Fig. 11. Here, lowering of temperature leads towards formation of shoulder around  $1.5a_B$  which is due to the formation of hydrogen atoms. This conclusion is confirmed by inspection of the corresponding quasibound electron trajectories as discussed above. At this temperature, the observed most probable electron distance is not  $1a_B$  as in the hydrogen ground state which is due to the considerable kinetic energy of the particles leading to a larger average radius of the classical quasiclosed orbits. We expect that at lower temperature, the most probable radius would tend towards  $1a_B$ , but this temperature range is not realistically modeled due to molecule and cluster formation.

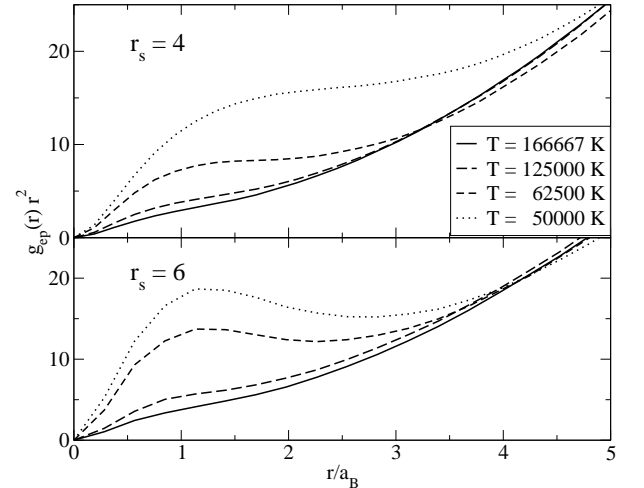


Figure 11: Electron-proton radial pair distribution functions multiplied by  $r^2$ . Same data as in Fig. 10.

While the description of correlated complexes of more than two particles is certainly beyond the present pair approximation model, nevertheless, several features of a partially ionized and partially dissociated hydrogen plasma are reproduced correctly. At 62 500 K and  $r_s = 6$  (right center part of Fig. 9) the simulations show a first weak signature of molecule formation – see the maximum of the p-p pair distribution function around  $r = 2a_B$  and the maximum of the pair distribution function of electrons with antiparallel spins around  $r = 1.5a_B$ . Further lowering of the temperature by a factor of two (lower panel of Fig. 9) confirms this trend: the p-p functions exhibit a clear peak very close to  $r = 1.4a_B$  – the theoretical p-p separation in  $H_2$ -molecules. At the same time, also the e-e functions have a clear peak around  $r = 0.5a_B$ , in the case of opposite spins, and  $r = 1.2a_B$ , for parallel spin projections. The first case comes rather close to the true quantum mechanical  $H - H$  bound state (singlet) with the electron wave function predominantly concentrated between the two protons. On the other hand, this electron peak should also extend to the right of the p-p peak, and no such pronounced peak would be expected for electrons with the same spin.

Nevertheless, we may conclude that even formation and spatial dimension of hydrogen molecules appear to be captured surprisingly well in these simulations. The main difficulty appears to arise not on the level of four-particle correlations but on the level of six particle correlations: in the simulations nothing prevents two “bound” atoms from binding to a third and more atoms. The overall attractive Coulomb interaction makes it, below 50,000 K, energetically favorable to form large clusters consisting of more than two atoms, explaining the strong decrease of the internal energy at the  $T = 31\,250$  K, cf. Fig. 8. In reality, complexes of two molecules do exist, but they have a very low binding energy which is due to a subtle compensation effects arising from repulsive exchange interaction between the electrons which go far beyond the level of pair interactions [45].

## VI. USE OF THE QUANTUM PAIR POTENTIALS IN DENSITY FUNCTIONAL THEORY

The effective quantum potentials have been introduced to represent the equilibrium two particle density matrix and subsequently generalized to incorporate many-body Coulomb coupling effects. There are other many body coupling effects due to degeneracy or exchange correlations. For some applications, it may be useful to incorporate these directly in the effective pair potentials to extend their validity to still lower temperatures, as was demonstrated on the example of classical MD above.

In this section, we describe the usefulness of the effective quantum potentials for a completely different theoretical approach – density functional theory (DFT). In doing so, the role of effective quantum potentials with degeneracy effects is illustrated as well.

DFT is a formal structure in which non-perturbative approximations can be introduced to describe strong coupling effects [47]. Although there are both classical and quantum versions of DFT, the classical form does not apply to a system of electrons and positive ions due to the Coulomb divergence. One possibility is to postulate a classical statistical mechanics using the effective quantum potentials described above which allows to remove the singularity. Alternatively, the proper quantum formulation can be used from the outset and the effective quantum potentials “derived” as a tool in the process of computing properties of interest [46]. This second approach will be used here.

In essence, DFT is a variational means to derive an equation for the charge density induced by an external potential. If that potential is taken to be the same as the potential of one of the charges in the system, the resulting density is in fact formally identical to the equilibrium pair correlation function, or diagonal element of the two particle density matrix. The density obeys a known nonlinear integral equation – a generalization of the Boltzmann-Poisson equation. However, in practice, the direct solution this equation is seldom attempted. Instead an equivalent set of self-consistent one particle Schrödinger equations, the Kohn-Sham equations [48], are solved first to construct the charge density. Yet it might be very useful to recall the existence of an alternative direct approach which becomes practical if an appropriate quantum pair potential is introduced. This is illustrated in more detail as follows.

Consider a quantum system in the presence of external sources that can be described by an additive potential

$$\hat{V} = \sum_{\alpha} \sum_{i=1}^{N_{\alpha}} \hat{V}_{\alpha}(\mathbf{q}_{i\alpha}). \quad (37)$$

Here  $\alpha$  denotes a species and  $\mathbf{q}_{i\alpha}$  is the position operator of particle  $i$  of species  $\alpha$ . The caret on the potentials is used to distinguish the quantum operator from its corresponding function. In general, each species may have a different form for the coupling to the external sources. The potential also can be written in terms of the density operators for each species

$$\hat{V} = \int d\mathbf{r} \sum_{\alpha} V_{\alpha}(\mathbf{r}) \hat{n}_{\alpha}(\mathbf{r}), \quad \hat{n}_{\alpha}(\mathbf{r}) = \sum_{i=1}^{N_{\alpha}} \delta(\mathbf{r} - \mathbf{q}_{i\alpha}). \quad (38)$$

The details of the remainder of the Hamiltonian are not important at this point. For this many-body system with external sources the theorems of density functional theory apply in the following form. First, a functional of the average densities,  $\hat{n}_{\alpha}(\mathbf{r})$ , averaged over an equilibrium

grand canonical ensemble is constructed (the generalization to other equilibrium ensembles has been carried out). This is done in two steps. First, the equilibrium grand potential for the system is considered formally

$$\beta\Omega_e = -\ln \sum_{\{n_\alpha\}} \text{Tr} e^{-\beta(H - \sum_\alpha \mu_\alpha n_\alpha)}. \quad (39)$$

The density for the various species is obtained (formally) by functional differentiation with respect to the potentials

$$\Omega_e = \Omega_e(\{\mu_\alpha - V_\alpha\}), \quad n_{e\alpha}(r) = -\frac{\delta\Omega_e}{\delta[\mu_\alpha - V_\alpha(r)]}. \quad (40)$$

The density equation is inverted (formally) to get the external potentials as functionals of the average densities

$$V_\alpha = \mathcal{V}_\alpha(\mathbf{r} | \{n_{e\sigma}\}), \quad (41)$$

and a Legendre transformation is performed to construct the free energy as a functional of the densities rather than the chemical potentials

$$F(\{n_{e\alpha}\}) = \Omega_e(\{\mu_\alpha - \mathcal{V}_\alpha\}) + \sum_\alpha \int d\mathbf{r} [\mu_\alpha - \mathcal{V}_\alpha(\mathbf{r} | \{n_{e\sigma}\})] n_{e\alpha}(\mathbf{r}). \quad (42)$$

The crucial second step is to extend this functional to *arbitrary density fields*

$$F(\{n_{e\alpha}\}) \rightarrow F(\{n\}). \quad (43)$$

The main task of density functional theory is now to construct the density functional

$$\Omega_V(\{n\}) \equiv F(\{n\}) - \int d\mathbf{r} (\mu_\alpha - V_\alpha(\mathbf{r})) n_\alpha(\mathbf{r}), \quad (44)$$

where, in this definition,  $V_\alpha(\mathbf{r})$  is *not* considered to be a functional of the density. The main theorem of density functional theory is then that this functional has an extremum at the equilibrium density

$$\frac{\delta\Omega_V(\{n\})}{\delta n} = 0 = \frac{\delta F(\{n\})}{\delta n} - [\mu_\alpha - V_\alpha(\mathbf{r})], \quad \Rightarrow n = n_{e\alpha}. \quad (45)$$

Furthermore the value of the functional at the equilibrium density is clearly the equilibrium grand potential

$$\Omega_V(\{n\}) = \Omega(\{\mu_\alpha - \mathcal{V}_\alpha\}).$$

In practice, an approximate free energy functional  $F(\{n\})$  is written and Eq. (45) is solved to obtain the equilibrium density. This density is then used to evaluate the equilibrium grand potential and determine all equilibrium thermodynamic properties. Structural properties can be obtained as well by choosing the external potential at the end to be the same as that for interaction

among the system particles. In other words, the source is chosen to be a particle of the same type as those comprising the many-body system. The densities  $n_{e\alpha}$  become equilibrium pair correlation functions.

How should the functional  $F(\{n\})$  be constructed? There is clearly a part associated with an ideal gas, and an energy due to the direct Coulomb interactions. These can be identified explicitly. In addition there are the more difficult parts due to exchange and correlations. Consequently, it has become standard practice to write the free energy as

$$F[n] = F^{(0)}(\{n\}) + \frac{1}{2} \sum_{\alpha,\sigma} \int d\mathbf{r} d\mathbf{r}' V_{\alpha\sigma}(\mathbf{r} - \mathbf{r}') n_\alpha(\mathbf{r}) n_\sigma(\mathbf{r}') + F_{xc}(\{n\}), \quad (46)$$

where  $F^{(0)}(\{n\})$  is the free energy for the non-interacting system, the second term is the contribution from the direct Coulomb interaction, and  $F_{xc}(\{n\})$  denotes the remaining contributions due to interactions from exchange and correlations. Then the extremum condition (45) becomes [46]

$$\mathcal{V}_\alpha^{(0)}(\mathbf{r} | \{n_\sigma\}) = V_\alpha(\mathbf{r}) + \sum_\sigma \int d\mathbf{r} d\mathbf{r}' V_{\alpha\sigma}(\mathbf{r} - \mathbf{r}') n_\sigma(\mathbf{r}') + \frac{\delta F_{xc}(\{n\})}{\delta n_\alpha(\mathbf{r})}, \quad (47)$$

with  $\mathcal{V}_\alpha^{(0)}(\mathbf{r} | n)$  denoting the functional (41) for the ideal gas. Determination of this functional is the central issue of the discussion here, and we will show that it is closely related to the Kelbg potential analyzed in the bulk of this paper.

The definition of the functional  $\mathcal{V}_\alpha^{(0)}(\mathbf{r} | n)$  is straightforward from the representation of the density for an *ideal Fermi gas* in the external potentials

$$n_\alpha(r) = \langle r | \left( e^{\beta \left( \frac{p^2}{2m_\alpha} + \hat{V}_\alpha - \mu_\alpha \right)} + 1 \right)^{-1} | r \rangle. \quad (48)$$

This is a single particle problem. The right side is clearly a functional of  $V_\alpha$  through the dependence of the eigenvalues of  $\frac{p^2}{2m_\alpha} + \hat{V}_\alpha$  on the form of the external potential. Interestingly, even at the level of the ideal gas determination of this functional is non-trivial. In the *non-degenerate limit* this equation for the density becomes

$$n_\alpha(r) \rightarrow \langle r | e^{-\beta \left( \frac{p^2}{2m_\alpha} + \hat{V}_\alpha - \mu_\alpha \right)} | r \rangle. \quad (49)$$

If the external potential is chosen to be a Coulomb source, then (49) becomes equivalent to the diagonal elements of the two particle density matrix in relative coordinates which has exactly the form of the pair distribution function used to define the effective quantum pair potential, cf. Eq. (21).

Once the exchange and correlation free energy functional is specified (guessed), (47) provides a set of closed *classical* integral equations for the equilibrium densities.

As will be seen below, a leading approximation is the usual Boltzmann-Poisson representation in terms of semi-classical potentials. The primary technical difficulty in this prescription is the determination of  $\mathcal{V}_\alpha^{(0)}(\mathbf{r} | n)$ . Kohn and Sham noted that (47) defines an effective single particle potential and therefore is formally equivalent to the ideal gas in this effective potential. Therefore, the solution can be constructed by solving the one particle Schrödinger equation whose potential is the right side of (47), and calculating the densities from the associated form (48) self-consistently

$$\begin{aligned} n_\alpha(r) &= \langle r | \left( e^{\beta \left( \frac{p^2}{2m_\alpha} + \hat{V}_\alpha - \mu_\alpha \right)} + 1 \right)^{-1} | r \rangle \\ &= \sum_i \left( e^{\beta(\epsilon_{i\alpha} - \mu_\alpha)} + 1 \right)^{-1} |\psi_i(r)|^2. \end{aligned} \quad (50)$$

This avoids the difficult problem of finding the functional  $\mathcal{V}_\alpha^{(0)}(\mathbf{r} | n)$  but at the cost of having to solve a set of self-consistent Schrödinger equations.

Consider instead an approximate evaluation of the potential  $\mathcal{V}_\alpha^{(0)}(\mathbf{r} | n)$  in terms of an effective quantum potential  $U_\alpha(r)$  defined by

$$\begin{aligned} n_\alpha(r) &\equiv \int \frac{d\mathbf{p}}{(2\pi\hbar)^3} \left( e^{\beta \left( \frac{p^2}{2m_\alpha} + U_\alpha(r) - \mu_\alpha \right)} + 1 \right)^{-1} \\ &= \langle r | \left( e^{\beta \left( \frac{p^2}{2m_\alpha} + \hat{V}_\alpha^{(0)} - \mu_\alpha \right)} + 1 \right)^{-1} | r \rangle. \end{aligned} \quad (51)$$

The first equality is similar to a finite temperature Thomas-Fermi representation, with a local chemical potential given by  $\mu_\alpha(r) = \mu_\alpha - U_\alpha(r)$ . An important difference discussed below is that  $U_\alpha(r) \neq V_\alpha(r)$ . The functional relationship of  $n_\alpha(r)$  to  $\mu_\alpha(r)$  and hence to  $U_\alpha(r)$  is that for an ideal gas and is well-known. The second equality of (51) defines the semi-classical potential  $U_\alpha(r | \mathcal{V}_\alpha^{(0)})$  as a functional of  $\mathcal{V}_\alpha^{(0)}$ . This relationship of  $U_\alpha(r | \mathcal{V}_\alpha^{(0)})$  to  $\mathcal{V}_\alpha^{(0)}$  is more difficult to unfold. However, it is straightforward to discover it for weak coupling of the system to the perturbing potential. The analysis is similar to the derivation of the Kelbg potential and will not be repeated here. Formally make the replacement  $\hat{\mathcal{V}}_\alpha^{(0)} \rightarrow \lambda \hat{\mathcal{V}}_\alpha^{(0)}$  in (51) with the corresponding dependence on  $\lambda$  inherited by  $U_\alpha(r)$ . Then perform the expansion of  $U_\alpha(r)$  to first order in  $\lambda$ , setting  $\lambda = 1$  at the end, to get [46]

$$U_\alpha(r) \rightarrow \int d\mathbf{r}' \pi_\alpha(\mathbf{r} - \mathbf{r}') \mathcal{V}_\alpha^{(0)}(\mathbf{r}') \quad (52)$$

where  $\pi_\alpha(\mathbf{r}, \mathbf{r}')$  is the well-known static linear polarization function in random phase approximation,

$$\pi_\alpha(\mathbf{r}) = (2\pi)^{-3} \int d\mathbf{r} e^{i\mathbf{k} \cdot \mathbf{r}} \tilde{\pi}_\alpha(k), \quad (53)$$

$$\tilde{\pi}_\alpha(k) = \frac{\partial \mu_\alpha}{\partial n_\alpha} \int \frac{d\mathbf{p}}{(2\pi\hbar)^3} \frac{F_\alpha(\mathbf{p} - \hbar\mathbf{k}) - F_\alpha(\mathbf{p})}{p^2 - (\mathbf{p} - \hbar\mathbf{k})^2}, \quad (54)$$

containing the Fermi distribution

$$F_\alpha(p) = \left( e^{\beta \left( \frac{p^2}{2m_\alpha} - \mu_\alpha \right)} + 1 \right)^{-1}. \quad (55)$$

In this approximation, the functional relationship between the density and the potential is now known

$$n_i(r) \equiv \int \frac{d\mathbf{p}}{(2\pi\hbar)^3} \left( e^{\beta \left( \frac{p^2}{2m_i} + \int d\mathbf{r}' \pi(\mathbf{r} - \mathbf{r}') \mathcal{V}_i^{(0)}(r') - \mu_i \right)} + 1 \right)^{-1} \quad (56)$$

Now it is straightforward to improve this results by substitution of (47) into the right side of (56) which gives a generalization of the Thomas-Fermi approximation to include strong coupling effects. However, even if  $F_{xc}(\{n\})$  is neglected the result is the Thomas-Fermi approximation in terms of the potential

$$\bar{V}_\alpha(\mathbf{r}) = \int d\mathbf{r}' \pi_\alpha(\mathbf{r} - \mathbf{r}') V_\alpha(\mathbf{r}') \quad (57)$$

rather than the bare potential  $V_\alpha(\mathbf{r})$ , which has short ranged divergences for opposite charge interactions. The result here in terms of the *nonlocal effective quantum potential* appears to be a new one that cures some of the well-known problems of the “local approximation” Thomas-Fermi theory. As indicated below,  $\bar{V}_\alpha(\mathbf{r})$  becomes just the Kelbg potential in the non-degenerate limit. The result (56) with (47) is a non-linear integral equation for the density, including both *strong coupling and degeneracy effects*. There is no longer any need to solve the Kohn-Sham equations and the problem is one of purely classical analysis.

It is instructive to consider the non-degenerate limit. In that case the polarization function is evaluated using  $F_0(p) \rightarrow e^{-\beta \left( \frac{p^2}{2m_\alpha} - \mu_\alpha \right)}$ . Furthermore, Eq. (56) simplifies to

$$n_\alpha(r) = n_\alpha e^{-\beta U_\alpha(r)}, \quad (58)$$

$$\mathcal{V}_\alpha^{(0)}(r') = \int d\mathbf{r}' \pi_\alpha^{-1}(\mathbf{r} - \mathbf{r}') U_\alpha(r'). \quad (59)$$

Use of these in the DFT equation (47) gives the closed equation for the densities

$$\begin{aligned} \ln \frac{n_\alpha(r)}{n_\alpha} &= -\beta \bar{V}_\alpha(\mathbf{r}) - \beta \sum_\sigma \int d\mathbf{r} d\mathbf{r}' \bar{V}_{\alpha\sigma}(\mathbf{r} - \mathbf{r}') n_\sigma(\mathbf{r}') \\ &+ \int d\mathbf{r}' \pi_\alpha(\mathbf{r} - \mathbf{r}') \frac{\delta F_{xc}(\{n\})}{\delta n_\alpha(\mathbf{r}')}. \end{aligned} \quad (60)$$

The potentials  $\bar{V}_\alpha(\mathbf{r})$  and  $\bar{V}_{\alpha\sigma}(\mathbf{r} - \mathbf{r}')$  are “regularized” by the polarization function, e.g.,

$$\bar{V}_\alpha(\mathbf{r}) = \int d\mathbf{r}' \pi_\alpha(\mathbf{r} - \mathbf{r}') V_\alpha(\mathbf{r}'). \quad (61)$$

It is possible to show [49] that in this *non-degenerate limit*  $\bar{V}_\alpha(\mathbf{r})$  is just the original Kelbg potential, Eq. (4).

Therefore, in the weak coupling limit where  $F_{xc}(\{n\})$  can be neglected (60) becomes the usual Boltzmann-Poisson equation with effective quantum potentials given by the Kelbg potential (4).

In summary, DFT applications can be performed in a semi-classical form without solving the Kohn-Sham equations by introducing effective quantum potentials. This can be done in a weak coupling approximation similar to that first described by Kelbg and yields a closed analytical result (4). Based on the results of the above analysis, it can be expected that this approach can be extended by incorporating as well effects of degeneracy by using for the density Eq. (48) instead of (58). Furthermore by using *improved quantum pair potentials* – along the lines of the improved Kelbg potentials discussed in the previous sections – an accurate treatment of the pair problem is achieved laying the foundation for advancing DFT to the regime of strong coupling.

## VII. DISCUSSION

In this work we presented an analysis of generalized quantum pair potentials. Extending the work of Kelbg and others we derived the effective off-diagonal and diagonal quantum pair potentials for a correlated hydrogen plasma including spin effects. These potentials have been used in path integral Monte Carlo and ‘semiclassical’ molecular dynamics simulations.

We investigated the accuracy of these potentials by detailed comparisons with the exact solutions of the Bloch equation. One important conclusion, of relevance to PIMC simulations, is that the off-diagonal potential gives essentially more accurate results (or more rapid con-

vergence) than its diagonal limit, quantitative estimates have been provided.

Further, we proceeded to derive improved diagonal quantum pair potentials by correcting the value of the Kelbg potential at zero particle separation. Comparison to the exact solutions of the two-particle Bloch equations allowed us to introduce a single temperature-dependent fit parameter. This lead to significantly improved diagonal pair potentials which are explicitly spin-dependent and still have the advantage of a closed analytical expression. These potentials have been shown to correctly reproduce thermodynamic quantities, such as total energies. Moreover, they can easily be used in ‘semiclassical’ molecular dynamics simulations of partially ionized plasmas up to moderate coupling (limited to temperatures above the molecule binding energy).

Finally an intimate relation of the quantum potentials to density functional theory has been explored which allows for DFT calculations without the need to solve the Kohn-Sham equations.

## VIII. ACKNOWLEDGMENTS

We acknowledge stimulating discussions with V. Filinov, W.D. Kraeft, D. Kremp and M. Schlanges. M.B. gratefully acknowledges hospitality of the Physics Department of the University of Florida.

This work has been supported by the Deutsche Forschungsgemeinschaft (BO-1366/2), the National Science Foundation and the Department of Energy (grants DE FG03-98DP00218 and DE FG02ER54677), as well as by grants for CPU time at the NIC Jülich and the Rostock Linux-Cluster “Fermion”.

- 
- [1] *Strongly Coupled Coulomb Systems*, G. Kalman (ed.), Pergamon Press 1998
  - [2] *Proceedings of the International Conference on Strongly Coupled Plasmas*, W.D. Kraeft and M. Schlanges (eds.), World Scientific, Singapore 1996
  - [3] W.D. Kraeft, D. Kremp, W. Ebeling, and G. Röpke, *Quantum Statistics of Charged Particle Systems*, Akademie-Verlag Berlin 1986
  - [4] M. Bonitz, “Quantum Kinetic Theory”, B.G. Teubner, Stuttgart/Leipzig 1998
  - [5] H. Haberland, M. Schlanges, W. Ebeling (eds.): Proc. 10th Int. Workshop on the Physics of Nonideal Plasmas, Contrib. Plasma Phys. **41**, No 2-3 (2001).
  - [6] “*Progress in Nonequilibrium Greens Functions*”, M. Bonitz (ed.), World Scientific Publ., Singapore 2000.
  - [7] L.B. Da Silva et al., Phys. Rev. Lett. **78**, 483 (1997).
  - [8] S.T. Weir, A.C. Mitchell, and W.J. Nellis, Phys. Rev. Lett. **76**, 1860 (1996)
  - [9] G.E. Norman, and A.N. Starostin, Teplofiz. Vys. Temp. **6**, 410 (1968); **8**, 413 (1970), [Sov. Phys. High Temp. **6**, 394 (1968); **8**, 381 (1970)]
  - [10] P. Haronska, D. Kremp, and M. Schlanges, Wiss. Z. Universität Rostock **98**, 1 (1987)
  - [11] D. Saumon, and G. Chabrier, Phys. Rev. A **44**, 5122 (1991)
  - [12] M. Schlanges, M. Bonitz, and A. Tschentschjan, Contrib. Plasma Phys. **35**, 109 (1995)
  - [13] D. Beule et al., Phys. Rev. B **59**, 14177 (1999); Contrib. Plasma Phys. **39**, 21 (1999)
  - [14] V.S. Filinov, V.E. Fortov, M. Bonitz, and P.R. Levashov, JETP Lett. **74**, 384 (2001) [Pis'ma v ZhETF **74**, 422 (2001)]
  - [15] W. Ebeling, W.D. Kraeft, and D. Kremp, “Theory of bound states and ionization equilibrium in plasmas and solids”. Akademie-Verlag Berlin 1976; Russ. Transl. Mir Moscow 1979
  - [16] D. Klakow, C. Toepffer, and P.-G. Reinhard, Phys. Lett. A **192**, 55 (1994); J. Chem. Phys. **101**, 10766 (1994).
  - [17] V. Golubnychiy, M. Bonitz, D. Kremp, and M. Schlanges, Phys. Rev. E **64**, 016409 (2001)
  - [18] For completeness we mention interesting concepts of quantum MD, such as wave packet MD, e.g. [16] and Wigner function MD [19], which are, however, beyond



the scope of this paper.

- [19] V.S. Filinov, P. Thomas, I. Varga, T. Meier, M. Bonitz, V.E. Fortov, and S.W. Koch, Phys. Rev. B **65**, 165124 (2002)
- [20] G. Kelbg, Ann. Physik, **12**, 219 (1963); **13**, 354; **14**, 394 (1964)
- [21] C. Deutsch, Phys. Lett. **60A**, 317 (1977)
- [22] F.J. Rogers, Phys. Rev. A **23**, 1008 (1981)
- [23] M.-M. Gombert, H. Minoo, and C. Deutsch, Phys. Rev. A **29**, 940 (1984)
- [24] F. Perrot and M.W.C. Dharma-wardana, Phys. Rev. B **62**, 16536 (2000)
- [25] J.-P. Hansen, P. Viellefosse, Phys. Lett. A, **53**, 187 (1975); S. Galam, J.P. Hansen, Phys. Rev. A **14**, 816 (1976)
- [26] H.E. De Witt, in *Strongly Coupled Plasmas*, ed. G. Kalman, and P. Carini (Plenum N.Y.), 1978.
- [27] V.S. Filinov, M. Bonitz, and V.E. Fortov, JETP Letters **72**, 245 (2000)
- [28] V.S. Filinov, V.E. Fortov, M. Bonitz, and D. Kremp, Phys. Lett. A **274**, 228 (2000)
- [29] V.S. Filinov, M. Bonitz, W. Ebeling, and V.E. Fortov, Plasma Phys. Contr. Fusion **43**, 743 (2001)
- [30] A. Filinov, M. Bonitz, and W. Ebeling, J. Phys. A: Math. Gen. **36**, 5957 (2003)
- [31] R.G. Storer, J. Math. Phys. **9**, 964 (1968); A.D. Klemm, and R.G. Storer, Aust. J. Phys. **26**, 43 (1973)
- [32] A.A. Barker, J. Chem. Phys. **55**, 1751 (1971)
- [33] D.M. Ceperley, Rev. Mod. Phys. **65**, 279 (1995)
- [34] H. Kleinert, *Path Integrals in Quantum Mechanics, Statistics and Polymer Physics*, World Scientific, Second edition, 1995.
- [35] H. Kleinert, Phys. Rev. D **57**, 2264 (1998)
- [36] K. Rohde, G. Kelbg, W. Ebeling, Ann. Physik **21**, 1 (1968)
- [37] M.-M. Gombert, H. Minoo, Contrib. Plasma Phys. **29**, 355 (1989)
- [38] W. Ebeling, Ann. Physik (Leipzig) **21**, 315 (1968); **22**, 33, 383, 392 (1969); Physica **38**, 378 (1968); **40**, 290 (1968).
- [39] W. Ebeling, A. Förster, V. Fortov, V. Gryaznov, and A. Polishchuk, *Thermophysical properties of hot dense plasmas*, Teubner, Stuttgart-Leipzig 1991
- [40] H. Xu, and J.P. Hansen, Phys. Rev. E **57**, 211 (1998).
- [41] W. Ebeling, H.J. Hoffmann, and G. Kelbg, Contr. Plasma Phys. **7**, 233 (1967) and references therein.
- [42] H. Wagenknecht, W. Ebeling, and A. Förster, Contrib. Plasma Phys. **41**, 15 (2001) and references therein
- [43] B. Militzer, PhD thesis, University Illinois, (2000)
- [44] The analytical form of the Kelbg potential is not well suited to describe the interaction of electrons with parallel spin. Instead, a suitable analytical approximation is given by Eq. (24).
- [45] More details of the MD simulations are given in V. Golubnychiy, PhD thesis, Rostock University 2003
- [46] L. Zogaib and J. Dufty (to be published)
- [47] N.D. Mermin, Phys. Rev. **137**, A1441 (1965).
- [48] W. Kohn and L. Sham, Phys. Rev. **140**, A1133 (1965).
- [49] J.W. Dufty, unpublished